Strangeness production and hypernuclear formation in proton- and antiproton-induced reactions

Zhao-Qing Feng ●*

School of Physics and Optoelectronics, South China University of Technology, Guangzhou 510640, China

Strange particles and hyperfragments in collisions of antiprotons and protons on nuclei have been investigated systematically within a microscopic transport model. The hyperons are produced from the annihilation in antibaryon-baryon collisions and the strangeness exchange process in antiproton induced reactions. A coalescence approach is used to construct the primary hyperfragments in phase space and the statistical model is modified to describe the decay of hyperfragments via evaporating hyperon, neutron, charged particles, etc., in which the shell effect, binding energy, and root-mean-square radii are taken into account. It is found that the influence of the hyperon-nucleon interaction on the free Λ and Ξ^- production is negligible. However, the large hyperfragment yields are obvious with the attractive potential. The production of double strangeness hyperfragments is reduced below 1 μb in comparison to the yields of Λ hyperfragments with cross sections of 0.05–0.1 mb in antiproton induced reactions on ^{63}Cu at incident momenta of 1–5 GeV/c. The light hyperfragments are formed in the dynamical fragmentation process. The energy dependence of hyperfragment formation is weak once the incident energy is above the threshold energy for the hyperon production.

I. INTRODUCTION

In the past several decades, strangeness nuclear physics has been extensively investigated both in experiments and in theories on the issues of hypernuclear physics, nuclear equation of state (EOS), hadronic matter properties, chiral symmetry restoration, etc. Inclusion of the strangeness degree of freedom in a nucleus extends the research activities in nuclear physics, in particular regarding the hypernucleus and kaonic nucleus, hyperon-nucleon and hyperon-hyperon interactions, and probing the in-medium properties of hadrons [1–7]. Since the first observation of the Λ hypernuclide in nuclear multifragmentation reactions induced by cosmic rays in the 1950s [8], remarkable progress has been obtained in terrestrial laboratories toward producing hypernuclides via different reaction mechanisms, such as hadron (pion, $K^{\pm}$, proton, antiproton) induced reactions, bombarding the atomic nucleus with high-energy photons or electrons, and fragmentation reactions with high-energy heavy-ion collisions. The spectroscopy, lifetime, giant monopole resonance, cluster structure, and decay modes of hypernuclei were investigated [9–12]. Recently, the antihypernuclide $^{3}_{\Lambda}\overline{\text{H}}$ was found by the STAR Collaboration in relativistic heavy-ion collisions and its binding energy was measured for the first time for testing the CPT theorem [13]. With the establishment of high-intensity high-energy accelerators in the world, such as PANDA (Antiproton Annihilation at Darmstadt, Germany) [14], Super-FRS/NUSTAR at FAIR (GSI, Germany) [15], NICA (Dubna, Russia) [16], J-PARC (Japan) [17], HIAF (high-intensity Heavy-Ion Accelerator Facility, China) [18], etc., the hypernuclear physics is to be extended on the topics of isospin degree of freedom (neutron-rich/proton-rich hypernuclei), multiple strangeness nuclei, antihypernuclei, and high-density hadronic matter with strangeness. Hypernucleus production with antiprotons and high-energy protons has attracted much attention at PANDA and HIAF, respectively. Understanding the dynamics of hypernuclei is expected and will be helpful for the management of detector systems in experiments.

The kinematics and properties of hypernuclei are related to the reaction mechanism. Exotic hypernuclei with extreme isospin asymmetry might be created via heavy-ion collisions. However, antiproton and antikaon induced reactions are favorable for producing multiple strangeness hypernuclei, in particular in the domain of heavy mass. The dynamics of hypernuclei in antiproton-nucleus collisions is associated with the hyperon production in the annihilation and meson-baryon collisions and with the capture of hyperons in the fragmentation process. The formation mechanism of hypernuclei in heavy-ion collisions and hadron-induced reactions has been extensively investigated by several approaches, i.e., the statistical multifragmentation model (SMM) [19,20], statistical approach with a thermal source [21], and microscopic transport models such as Giessen Boltzmann-Uheling-Uhlenbeck (GiBUU) [22,23] and quantum molecular dynamics (QMD) [24–26]. The dynamical description of hypernucleus formation is still expected for evaluating the production cross section, the cluster effect in the preequilibrium process, correlation of the Λ-Λ interaction, etc.

In this work, the production mechanisms of strange particles and hypernuclei in proton- and antiproton-induced

*fengzhq@scut.edu.cn

reactions will be investigated within the Lanzhou quantum molecular dynamics (LQMD) transport model. The article is organized as follows. In Sec. II I give a brief description of the model. The calculated results and discussion are presented in Sec. III. A summary and perspective on the hypernuclear production are outlined in Sec. IV.

II. BRIEF DESCRIPTION OF THE THEORETICAL APPROACH

In the past several years, the LQMD transport model was developed to investigate the density dependence of symmetry energy, isospin splitting of nucleon effective mass and in-medium effects of hadrons in heavy-ion collisions, spallation reactions induced by hadrons, and the annihilation mechanism in antiproton-nucleus collisions. Recently, the model was modified to describe the formation mechanism of hypernuclei in heavy-ion collisions and in antikaon-induced reactions [27]. In the LQMD transport model, the dynamics of resonances with mass below 2 GeV [$\Delta(1232)$, $N^*(1440)$, $N^*(1535)$, etc], hyperons (Λ, Σ, Ξ), and mesons (π, η, K, $\overline{K}$, ρ, ω) is described by coupling the hadron-hadron collisions and rescattering processes via the decay reproduction of resonances, baryon-antibaryon annihilation reactions, and meson-baryon and baryon-baryon collisions [28,29]. The temporal evolutions of nucleons and nucleonic resonances are described by Hamilton's equations of motion under the self-consistently generated two-body and three-body interaction potentials with the Skyrme-like force. The one-body potentials of kaons (antikaons) and hyperons are used for transportation in nuclear medium and evaluated by the chiral effective Lagrangian approach and relativistic mean-field theories [30,31], respectively. The optical potential of the hyperon is written as

$$V_Y(\mathbf{p}, \rho) = \omega_Y(\mathbf{p}, \rho) - \sqrt{\mathbf{p}^2 + m^2}, \tag{1}$$

in which the in-medium energy is derived from

$$\omega_Y(\mathbf{p}_i, \rho_i) = \sqrt{\left(m_H + \Sigma_S^H\right)^2 + \mathbf{p}_i^2} + \Sigma_V^H. \tag{2}$$

The self-energies of hyperons are assumed to be two thirds of that experienced by nucleons, namely $\Sigma_S^\Lambda = 2\Sigma_S^N/3$, $\Sigma_V^\Lambda = 2\Sigma_V^N/3$, $\Sigma_S^\Xi = \Sigma_S^N/3$, and $\Sigma_V^\Xi = \Sigma_V^N/3$. The nucleon scalar Σ_S^N and vector Σ_V^N self-energies are computed from the well-known relativistic mean-field model with the NL3 parameter ($g_{\sigma N} = 8.99$, $g_{\omega N} = 12.45$, and $g_{\rho N} = 4.47$) [32]. The values of optical potentials at saturation density are -32 and -16 MeV for Λ and Ξ, respectively. A weakly repulsive ΣN potential with 12 MeV at saturation density is used by fitting the calculations of chiral effective field theory [33]. The hyperon-nucleon interaction potentials will influence the dynamics of hyperons in nuclear medium, i.e., kinetic energy spectra, emission anisotropy, etc. Furthermore, the bound states to form nuclear fragments and hypernuclei are modified by the potential.

The nuclear dynamics induced by low-energy antiprotons has been extensively investigated within the LQMD model, i.e., the strange particle production, preequilibrium nu-

cleon emission, fragmentation reactions, etc. The antiproton-nucleon potential influences the reaction dynamics and the hyperfragment formation, which is calculated by performing the G-parity transformation of nucleon self-energies. The optical potential of the antiproton in nuclear medium is derived from the in-medium energy as

$$V_{\overline{p}}(\mathbf{p}, \rho) = \omega_{\overline{N}}(\mathbf{p}, \rho) - \sqrt{\mathbf{p}^2 + m^2}. \tag{3}$$

The antinucleon energy in nuclear medium is evaluated by the dispersion relation as

$$\omega_{\overline{N}}(\mathbf{p}_i, \rho_i) = \sqrt{\left(m_N + \Sigma_S^{\overline{N}}\right)^2 + \mathbf{p}_i^2} + \Sigma_V^{\overline{N}} \tag{4}$$

with $\Sigma_S^{\overline{N}} = \xi \Sigma_S^N$ and $\Sigma_V^{\overline{N}} = -\xi \Sigma_V^N$ with $\xi = 0.25$. The strength of the optical potential $V_{\overline{N}} = -164$ MeV is obtained at the normal nuclear density $\rho_0 = 0.16$ fm^{-3} by fitting the available experimental data of antiproton-nucleus scattering.

The hadron-hadron collisions in elastic, inelastic scattering, and charge (strangeness) exchange reactions are performed with a Monte Carlo procedure and weighted by Pauli blocking of the final states. The choice of reaction channel is randomly performed by the weight of the channel probability, which is evaluated by comparing the channel to the total cross section. All possible channels of pseudoscalar mesons and hyperons in meson-baryon and baryon-baryon collisions are included to describe heavy-ion collisions and hadron (proton, $\pi^\pm$, $K^\pm$) induced reactions. To treat antiproton-nucleus collisions, the annihilation channels, charge-exchange reactions (CEX), elastic (EL) and inelastic scattering with antibaryons and hyperons with multiple strangeness are included as follows [25]:

$$\overline{B}B \to \text{annihilation}(\pi, \eta, \rho, \omega, K, \overline{K}, \eta', K^*, \overline{K}^*, \phi),$$

$$\overline{B}B \leftrightarrow \overline{B}B(\text{CEX,EL}), \quad \overline{N}N \leftrightarrow \overline{N}\Delta(\overline{\Delta}N), \quad \overline{B}B \leftrightarrow \overline{Y}Y,$$

$$\overline{B}B \leftrightarrow \overline{\Xi}\Xi, \quad \overline{K}B \leftrightarrow K\Xi, \quad YY \leftrightarrow N\Xi, \quad \overline{K}Y \leftrightarrow \pi\Xi. \tag{5}$$

Here the B stands for a nucleon and $\Delta(1232)$, Y (Λ, Σ), Ξ ($\Xi^{0,-}$), K (K^0, K^+), or $\overline{K}$ ($\overline{K}^0$, K^-). The overline of B (Y) means its antiparticle. Mesons are the main products in antiproton-induced reactions. Besides the strangeness exchange reactions such as $\overline{K}N \to \pi Y$, hyperons are also contributed from the meson-induced reactions $B\pi(\eta) \leftrightarrow YK$. The main products are pions with wide energy spectra in the antiproton-induced reactions. Therefore, hypernuclei might be produced with low-energy antiproton beams.

The fragments formed in the hadron-induced reactions are mainly distributed in the targetlike region. Once a hyperon is created, it might be captured by surrounding nuclear fragments to form a hypernucleus. The fragments are recognized with a coalescence model in phase space, in which the nucleons at freeze-out in nuclear collisions are considered to belong to one cluster with the relative momentum smaller than P_0 and with the relative distance smaller than R_0 (here $P_0 = 200$ MeV/c and $R_0 = 3$ fm). Actually, the influence of the coalescence parameters on the final fragments is small because the lager

coalescence distance increases the excitation energy of the primary fragment and enables the de\excitation process. The root-mean-square radii of the constructed fragment is checked with the normal radii-mass formula. The excitation energy is evaluated as the difference of binding energies between the excited fragment and the Bethe-Weizsäcker mass formula for nuclear fragments. The generalized mass formula with SU(6) symmetry breaking is used to calculate the hypernuclear binding energy [34]. The reaction system evolves until the excitation energy of 3A MeV with the mass number A of the fragment, at which point the nonequilibrium transportation is stopped and particle evaporation is dominant. The deexcitation process of the nuclear fragment and hyperfragments is described by the GEMINI code [35], in which the channels of γ, light complex clusters (n, p, α, etc.), and binary fragments are selected by a Monte Carlo procedure via the decay width. The decay widths of light particles with Z $\leqslant$ 2 and the binary decay are calculated by the Hauser-Feshbach formalism [36] and transition state formalism [37], respectively. The hyperon decay width is also evaluated by the Hauser-Feshbach approach the phenomenological hyperon binding energy. In the LQMD model, the binding energy of the primary fragment is calculated by the internal motion energy and interaction potential as

$$
\begin{aligned}
E_B(Z_i, N_i) = & \sum_j \sqrt{p_j^2 + m_j^2} - m_j \\
& + \frac{1}{2} \sum_{j,k,k \neq j} \int f_j(\mathbf{r}, \mathbf{p}, t) f_k(\mathbf{r}', \mathbf{p}', t) \\
& \times v(\mathbf{r}, \mathbf{r}', \mathbf{p}, \mathbf{p}') d\mathbf{r}\, d\mathbf{r}'\, d\mathbf{p}\, d\mathbf{p}' \\
& + \frac{1}{6} \sum_{j,k,l} \sum_{k \neq j, k \neq l, j \neq l} \int f_j(\mathbf{r}, \mathbf{p}, t) f_k(\mathbf{r}', \mathbf{p}', t) \\
& \times f_l(\mathbf{r}'', \mathbf{p}'', t) v(\mathbf{r}, \mathbf{r}', \mathbf{r}'', \mathbf{p}, \mathbf{p}', \mathbf{p}'') \\
& \times d\mathbf{r}\, d\mathbf{r}' d\mathbf{r}'' d\mathbf{p}\, d\mathbf{p}' d\mathbf{p}'',
\end{aligned} \tag{6}
$$

where the $\mathbf{r}, \mathbf{p}$ are the nucleon positions in the center of mass of the ith fragment (Z_i, N_i). The phase space density $f(\mathbf{r}, \mathbf{p}, t)$ is calculated with the QMD wave function. I count the binding energy of the hyperfragment as $E_B(Z_i, N_i, N_Y) = E_B(Z_i, N_i) + \sum_{j=1}^{N_Y} \omega(\mathbf{p}_j, \rho_j) - m_H$, with Z_i, N_i, and N_Y being the proton, neutron, and hyperon numbers, respectively. It is noticed that the combined approach of the coalescence method and statistical model is available for the medium and heavy fragments because of the reliable estimation of binding energy. In the hadron-induced reactions, the fragments are distributed in the targetlike region and the statistical decay is implemented only for the fragments with mass number $A >$ 12. The emissions of light clusters are complicated in nuclear collisions, and are related using dynamical recognition via the nucleon-nucleon scattering and the structure effect at freeze-out. Recently, a new approach, FRIGA (Fragment Recognition in General Application), was proposed to identify the nuclear fragments and hypernuclei in heavy-ion collisions [26], in which the shell effect and odd-even effect are taken into account in recognizing the fragments.

III. RESULTS AND DISCUSSION

Mesons, resonances, and hyperons produced in heavy-ion collisions and hadron-induced reactions are modified in the nuclear medium. The elementary cross section, decay width, effective mass, energy spectra, invariant decay channels, etc., have been extensively investigated [38,39]. The dynamics of hyperons is significant in the hyperfragment formation, which has been investigated to extract the high-density equation of state and the properties of hadronic matter formed in heavy-ion collisions. Shown in Fig. 1 is the influence of the optical potentials on the production of hyperons Λ and Ξ^- in collisions of $\bar{p}$ on ^{63}Cu at a beam momentum of 3 GeV/c. The Ξ^- production is strongly suppressed by three orders of magnitude in comparison to the Λ yields. The Λ-nucleon potential slightly changes the spectra. The Ξ^- yields are enhanced with the potential because of the reduction of threshold energy. Although the Λ potential increases its production, the reabsorption process $\pi\Lambda \rightarrow \bar{K}N$ weakens the Λ production owing to the abundant pions from antiproton annihilation.

The strange particles produced in antiproton-induced reactions are associated with the annihilation and secondary collisions. At incident momentum above the threshold energy, e.g., the reactions $\overline{N}N \rightarrow \bar{\Lambda}\Lambda$ ($p_{\text{threshold}} = 1.44$ GeV/c) and $\overline{N}N \rightarrow \overline{\Xi}\Xi$ ($p_{\text{threshold}} = 2.62$ GeV/c), the production of hyperons is attributed to the direct reaction [annihilation and creation of quark pairs, $u\bar{u}(d\bar{d}) \rightarrow s\bar{s}$] and also to the secondary collisions, i.e., meson-induced reactions $\pi(\eta, \rho, \omega)N \rightarrow KY$ and strangeness exchange reaction $\bar{K}N \rightarrow \pi Y(K\Xi)$. At momentum below the threshold energy, the strangeness exchange reactions and pion-nucleon collisions dominate the hyperon production. Shown in Fig. 2 are the invariant mass spectra of hyperons Λ and Ξ^- in collisions of $\bar{p}$ on ^{63}Cu at different momenta and on targets of ^{40}Ca, ^{63}Cu, ^{124}Sn, and ^{197}Au at a momentum of 3 GeV/c. The momentum dependence of hyperon yields is pronounced in the high kinetic energy region. The hyperons are contributed from the direct annihilation process at incident momentum above 3 GeV/c. The strangeness exchange reactions are obvious with increasing mass number of target nuclide owing to the higher collision probability between the meson and nucleon. The advantage of antiproton-induced reactions is the multichannel contributions for hyperon production, which is also available for hyperfragment formation.

The target nucleus is heated by incoming antiprotons via the annihilation reactions and the localized energy is released through the collisions of annihilation products and nucleons, which enables the formation of a highly excited nucleus. The energy deposition and spallation mechanisms in antiproton-induced reactions are still to be investigated. Shown in Fig. 3 is the excitation energy distribution in collisions of $\bar{p}$ on ^{63}Cu at beam momenta of 1, 2, 3, 4, and 5 GeV/c in the left panel, and in antiproton-induced reactions on ^{40}Ca, ^{63}Cu, ^{124}Sn, and ^{197}Au at 3 GeV/c. The collisions processes in antiproton-induced reactions include elastic scattering, annihilation, and secondary collisions with surrounding nucleons. The annihilation cross section decreases with increasing antiproton energy. Therefore, the large excitation energy is released from the multiple collisions between pions and nucleons at the incident
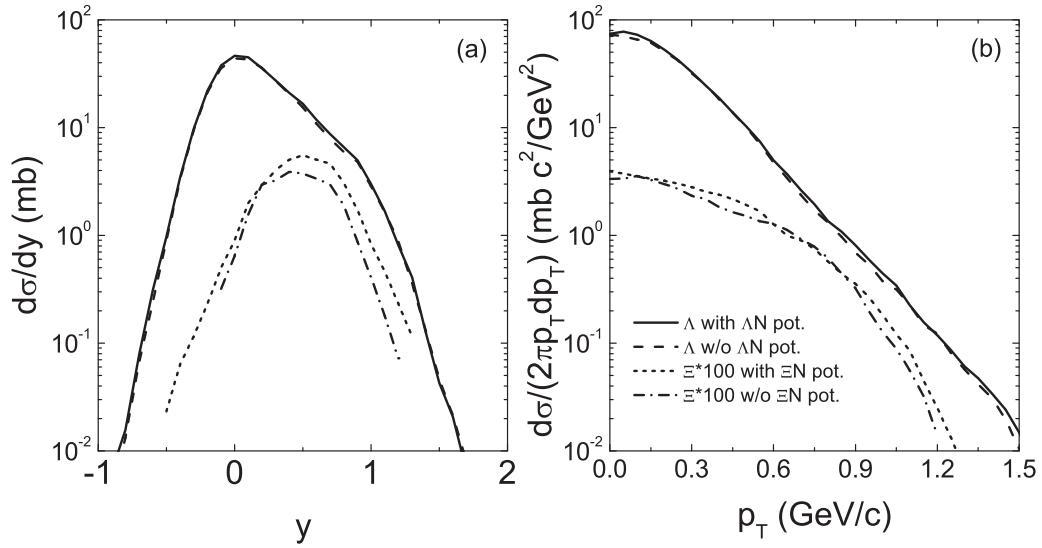
FIG. 1. Rapidity and transverse momentum spectra of Λ and Ξ^- produced in antiproton-induced reactions on ^{63}Cu at a beam momentum of 3 GeV/c.

momentum of 1 GeV/c. The energy dissipation is obvious in the heavy target nuclide and leads to the high excitation energy. The fragments formed in antiproton- and proton-induced reactions are positioned in the targetlike region. The nuclear dynamics induced by antiprotons and protons is described by the LQMD model. The primary fragments are constructed
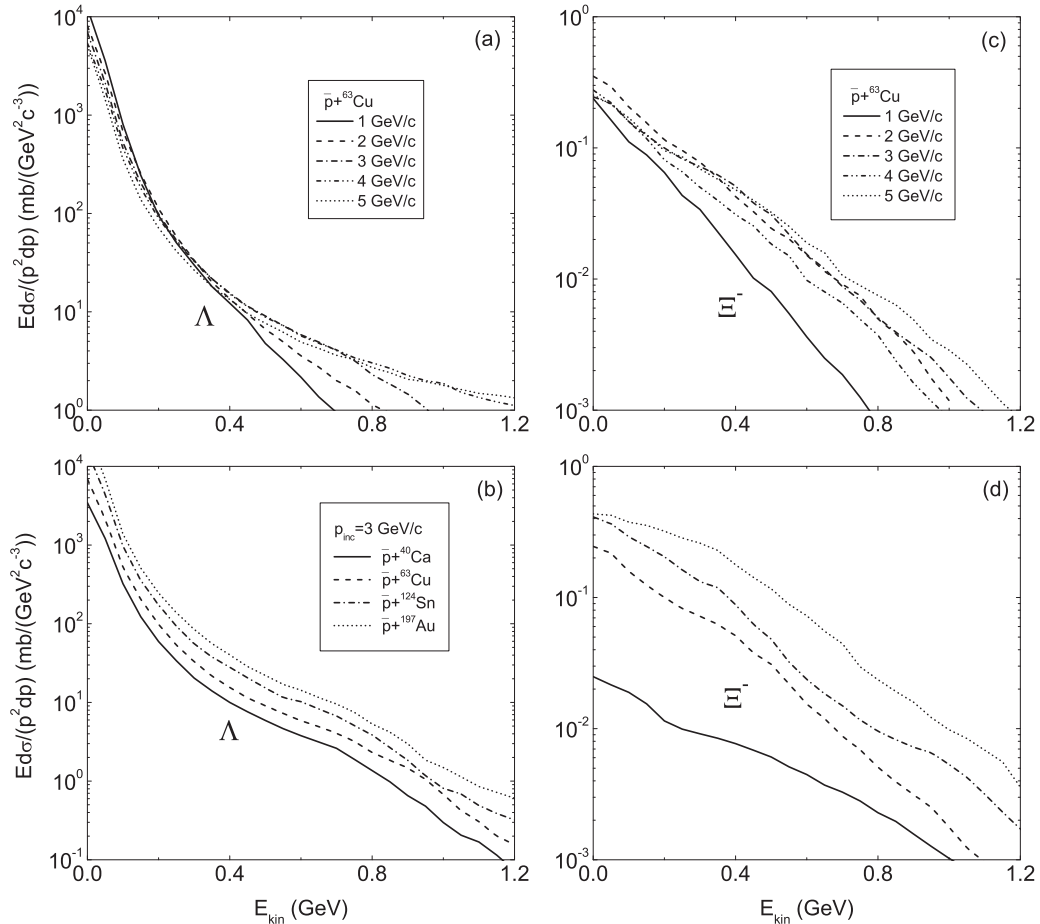
FIG. 2. Inclusive spectra of Λ and Ξ^- produced in $\bar{p} + {}^{63}$Cu at different energies and on different targets at a beam momentum of 3 GeV/c.
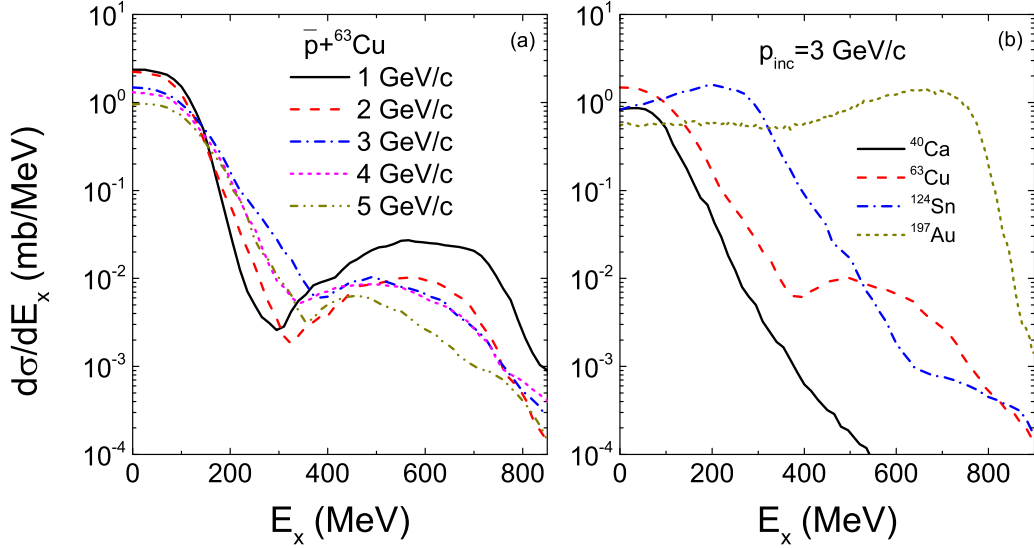
FIG. 3. Excitation energy distribution in antiproton-induced reactions with different systems and incident momenta.

with a coalescence model at freeze-out stage in the nuclear collisions, in which the particle yields reach equilibrium values. The primary fragments are highly excited and the deexcitations of the fragments are described by the statistical code. Shown in Fig. 4 is a comparison of the hyperon-nucleon potential and statistical decay of the hyperfragment production in the reaction $p + ^{63}$Cu at 5 GeV/c. It is obvious that the attractive hyperon-nucleon potential is favorable for hyperfragment formation. The relative momentum between the hyperon and nuclear cluster is reduced with the potential, which enables the hyperon capture to form a hypernuclide. Inclusion of the statistical decay in the primary fragments leads to a yield reduction of one order of magnitude.

The nuclear fragmentation reactions induced by antiprotons were extensively investigated in experiments with the LEAR (Low-Energy Antiproton Ring) facility at CERN, in

which some topical issues were taken into account, i.e., the preequilibrium emissions of nucleons and clusters, the delayed fission from the decay of hypernuclei, particle production, in-medium effects of hadrons, etc. [40–43]. Experimentally, the hypernuclei are reconstructed from the invariant mass spectra of π^- and its decay fragments. The kinematics of hyperfragments is helpful for detector management in experiments, i.e., the rapidity distribution, transverse (kinetic energy) spectra, invariant energy, angular emission, etc. The rapidity distributions of Λ hyperfragments produced in proton (5 GeV/c) and antiproton (2–5 GeV/c) induced reactions on ^{63}Cu are calculated as shown in Fig. 5. It is obvious that the light fragments are formed in the spallation process, which weakly depends on the incident momentum in the antiproton-induced reactions. The spectra manifest a symmetric structure with antiprotons. The
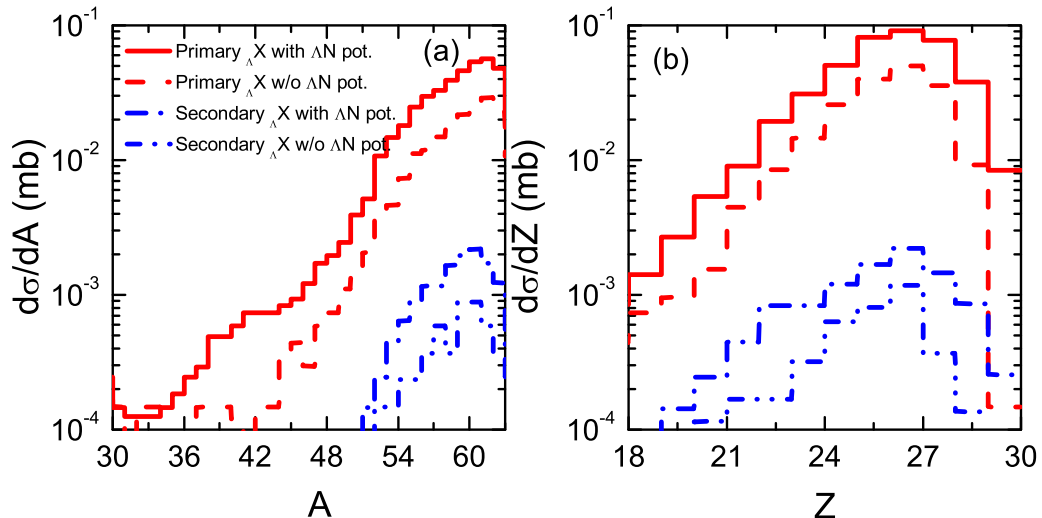

FIG. 4. Influence of the statistical decay and hyperon-nucleon potential on the hyperfragment formation in the reaction of protons on ^{63}Cu at an incident momentum of 5 GeV/c.
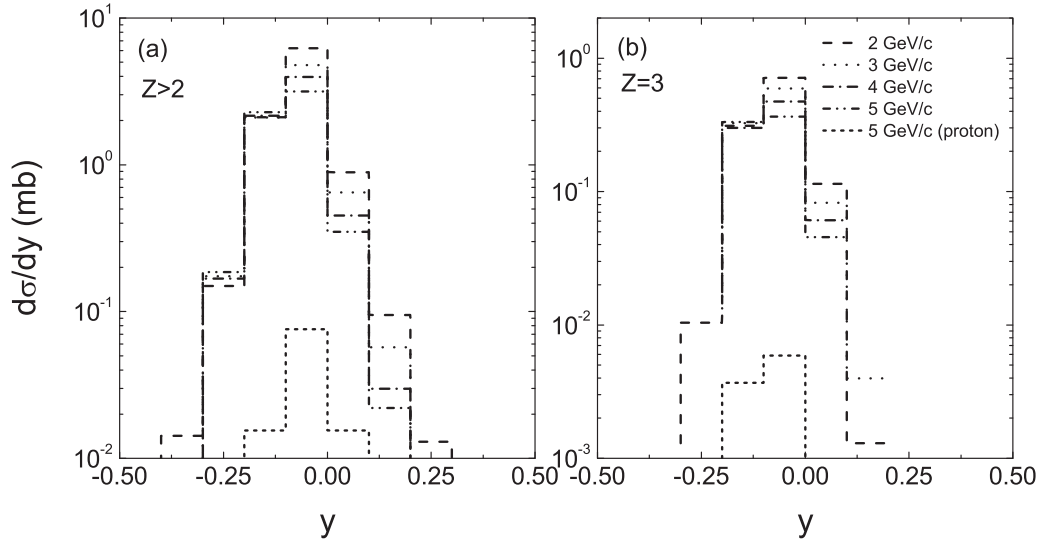
FIG. 5. Rapidity distribution of hyperfragments with $Z > 2$ and hyperlithium in collisions of antiprotons and protons on ^{63}Cu.

hypernuclear production is strongly suppressed in the proton-nucleus collisions.

Once a hyperon is created inside the nucleus, the relative momentum between the hyperon and nucleon might be reduced to form a hypernucleus owing to multiple collisions. This has advantages for creating heavy hypernuclei with the hadron-induced reactions in comparison to heavy-ion collisions. The fragments and hyperfragments tend to be formed around the β-stability line in the fragmentation process. The hyperon is produced in the antiproton-induced reactions at very low energies because of the contributions of meson-nucleon collisions and the strangeness exchange process, e.g., $\pi N \to K \Lambda$ ($p_{\text{threshold}} = 0.89$ GeV/c), $\overline{K} N \to \pi \Lambda$. The direct annihilation dominates the hyperon production at high energy, $\overline{N} N \to \overline{\Lambda} \Lambda$ ($p_{\text{threshold}} = 1.44$ GeV/c). Shown in Fig. 6 is a comparison of hyperfragments in the reaction $\overline{p} + {}^{63}$Cu at different momenta. At low incident momentum (1 GeV/c), more

temporal dissipation enables the high excitation energy, which leads to more nucleon or cluster emissions. Overall, the energy dependence of hyperfragment production is not obvious in the antiproton-induced reactions. The properties of double strangeness hypernuclei are of importance in exploring the Λ-Λ interaction, the three-body force of the $\Lambda\Lambda N$ state, short-range correlation, etc. The double Λ hypernucleus production at different incident momenta is calculated as shown in Fig. 7. The double strangeness hypernuclei are mainly contributed from the strangeness exchange reaction $N \Xi \to YY$. The dynamics of Ξ is of significance for hypernuclide formation. The hyperon Ξ is created via the annihilation reaction $\overline{p} N \to \overline{\Xi} \Xi$ above the antiproton threshold momentum $p_{\text{threshold}} = 2.62$ GeV/c and the secondary collision $\overline{K} N \to K \Xi$ above the antikaon threshold momentum $p_{\text{threshold}} = 1.04$ GeV/c. A small distance between the hyperon and nucleon in phase space is favorable for a bound hyperfragment. The max-
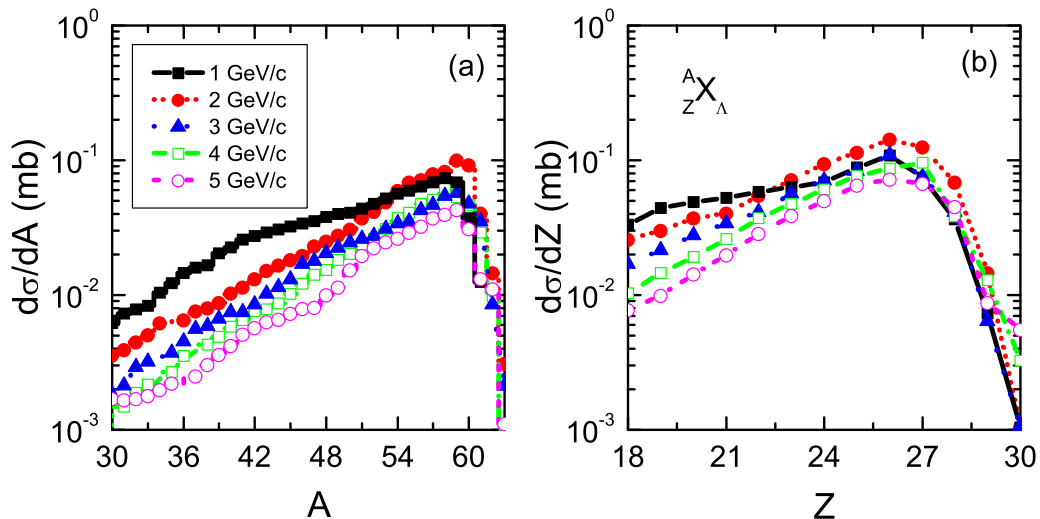

FIG. 6. Incident energy dependence of Λ hyperfragments as functions of mass and charge number in collisions of $\overline{p} + {}^{63}$Cu, respectively.
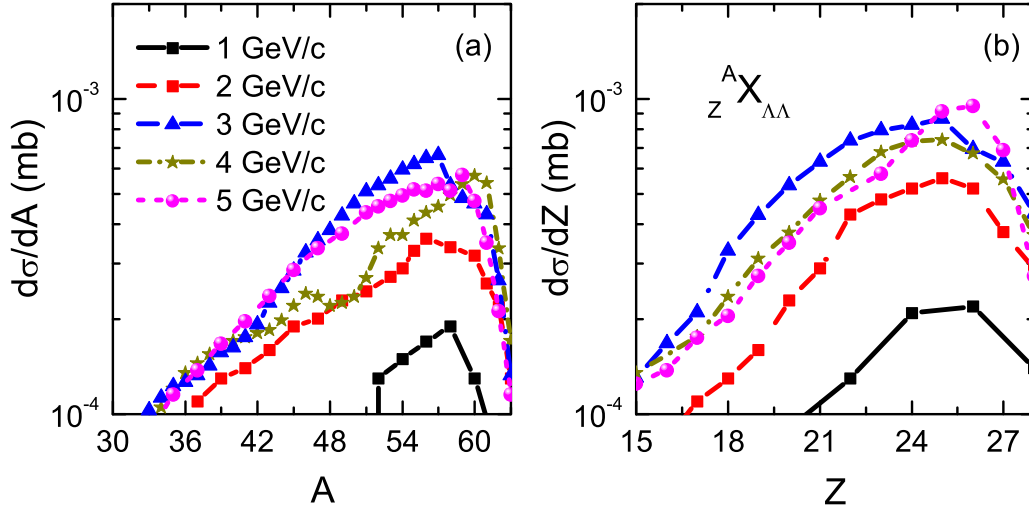
FIG. 7. Hyperfragment production with double strangeness in antiproton-induced reactions at different energies.

imal yields around 0.5–1 μb are found at momenta of 2–5 GeV/c, which are feasible for experimental measurements at PANDA (Antiproton Annihilation at Darmstadt, Germany) in the near future.

The spallation reactions induced by protons and antiprotons have been extensively investigated with different models, which are associated with the inequilibrium process leading to the fragmentation and excitation of colliding system and with the decay modes via evaporating γ rays, particles, and fission of heavy fragments. The SMM was applied to describe the multifragmentation and hypernucleus production. One needs to input the the mass, charge, hyperon numbers, and temperature for a composite system. Recently, combined approaches of the SMM and transport models have been used for hypernuclear production in heavy-ion collisions, i.e., UrQMD [44], the Dubna cascade model [45], and the GiBUU

model [46]. A comparison of the LQMD and GiBUU results for the antiproton-induced reactions is shown in Fig. 8. The thermal source and hadron dynamics in collisions of $\bar{p} + {}^{64}$Cu at a momentum of 5 GeV/c are provided by GiBUU and the hypernuclide production in the fragmentation is described by the SMM [47]. The experimental data from the LEAR facility at CERN [40] are shown for a comparison. The mass distribution of nuclear fragments is nicely consistent with the data. It is noticed that the shapes of charge and mass distributions in the antiproton-induced reactions weakly depend on the incident momentum, but strongly on the annihilation of antiprotons in a nucleus [25]. The normal nuclear fragments are almost consistent in both calculations. However, the Λ and $\Lambda\Lambda$ hyperfragments are reduced by about the one order magnitude with LQMD in comparison with the estimation by the GiBUU model. The possible reason is some hyperons
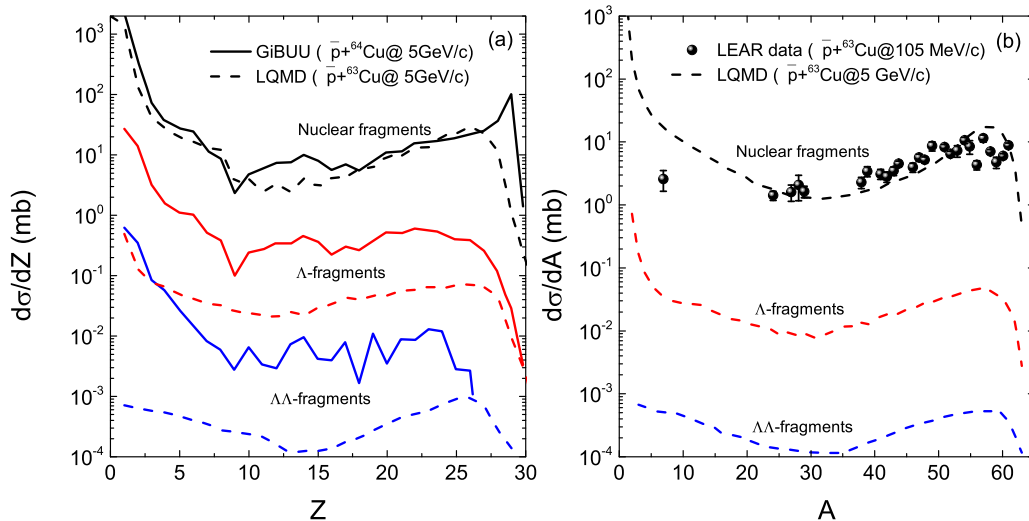

FIG. 8. Mass and charge distributions of fragments produced in the $\bar{p} + {}^{63}$Cu reaction at an incident momentum of 5 GeV/c. The calculations from the GiBUU model for $\bar{p} + {}^{64}$Cu at 5 GeV/c [47] and the available data from the LEAR facility at CERN [40] are shown for a comparison.
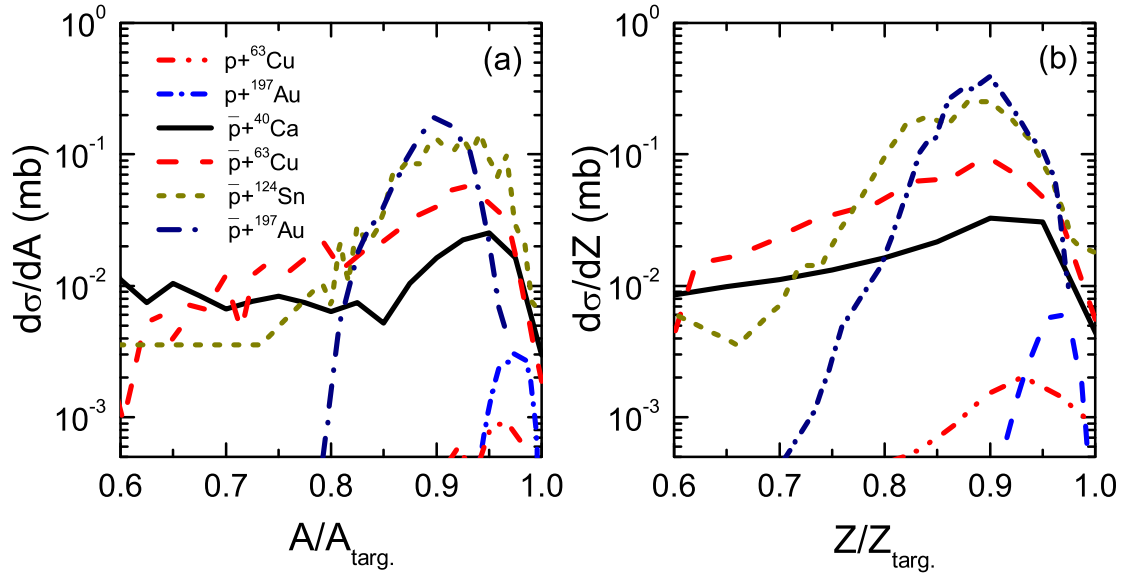
FIG. 9. Comparison of Λ-hyperfragment production with proton- and antiproton-induced reactions on different targets.

escaping the nuclear composite system in the collisions. Large yields appear in the targetlike regime and light fragments with the charge number $Z \leqslant 5$ in the LQMD calculations. However, a plateau is caused by the multifragmentatoin process in the combined GiBUU and SMM. More measurements of hyperfragments in the hadron (lepton) induced reactions and in heavy-ion collisions are expected to improve the theoretical description. The recognition method is also significant when evaluating the nuclear fragments and hyperfragments, such as in fragment recognition in general applications [26]. Besides the dynamical fragmentation and constructiion of fragments at freeze-out, the clusters in multiple collisions also need to be taken into account in the transport models. Further investigation of hyperfragment formation in multiple collisions and the dynamical recognition method is in progress.

The formation of hyperfragments in hadron-induced reactions is related to the reaction system. The energy relaxation is pronounced in heavy targets because of multiple-step collisions with surrounding nucleons, which influence the excitation magnitude and target fragmentation. Usually, the excitation energy increases with the mass of the target nucleus, and the fragmentation is also explosive. Shown in Fig. 9 is a comparison of the Λ hyperfragments in the proton-induced reactions on the targets ^{63}Cu and ^{197}Au at a momentum of 5 GeV/c, and antiprotons on ^{40}Ca, ^{63}Cu, ^{124}Sn, and ^{197}Au at 3 GeV/c. The antiproton beams are favorable for creating hypernuclei with maximal cross section above 0.01 mb and increase the yields by over two orders magnitude in comparison to the proton-induced reactions. Hypernucleus production with proton beams is feasible with cross section above 1 μb. Reactions induced by both proton and antiproton beams manifest the spallation mechanism, in which the yields of intermediate fragments (IMFs) are low. The fragments are

mainly distributed in the targetlike and light-mass domains. Experiments in hypernuclear physics with high-energy protons are planned at the HIAF facility in the near future.

IV. CONCLUSIONS

In summary, the dynamics of strange particles and hypernuclear production in proton- and antiproton-induced reactions have been investigated within the LQMD transport model. The hyperons Λ and Ξ^- are mainly created from strangeness exchange reactions, meson-nucleon collisions, and direct annihilations in collisions of antiprotons on a target nucleus. Nucleon-nucleon direct collisions contribute to hyperon production in proton-induced reactions. The hyperfragments are formed in the targetlike domain with hadron-induced reactions. The influence of the hyperon-nucleon potential on hyperon energy spectra is negligible, but favorable for hyperfragment formation. Inclusion of the statistical decay leads to one order-of-magnitude reduction of hyperfragments. The production cross sections of double strangeness hypernuclei with antiproton beams are found to be at the level of 1 μb, which is feasible for experiments at PANDA. The yields of hyperfragments are independent of the incident energy above the threshold energies in the annihilation reactions for direct hyperon production. Λ hyperfragments omfr high-energy proton beams might be measured at HIAF.

[1] B. F. Gibson and E. V. Hungerford III, Phys. Rep. **257**, 349 (1995).

[2] T. Falter, J. Lehr, U. Mosel, P. Muehlich, and M. Post, Prog. Part. Nucl. Phys. **53**, 25 (2004).

[3] O. Hashimoto and H. Tamura, Prog. Part. Nucl. Phys. **57**, 564 (2006).

[4] H. Lenske and M. Dhar, in *The Euroschool on Exotic Beams - Vol. 5*, edited by C. Scheidenberger and M. Pfützner, Lecture Notes in Physics Vol. 948 (Springer, Berlin, 2018), p.161; H. Lenske, M. Dhar, T. Gaitanos, and X. Cao, Prog. Part. Nucl. Phys. **98**, 119 (2018).

[5] E. Epple and L. Fabbietti, Phys. Rev. C **92**, 044002 (2015).

[6] Y. Sada *et al.*, Prog. Theor. Exp. Phys. **2016**, 051D01 (2016).

[7] R. Y. Yang, W. Z. Jiang, and S. N. Wei, Phys. Lett. B **795**, 188 (2019).

[8] M. Danysz and J. Pniewski, Philos. Mag. **44**, 348 (1953).

[9] K. Nakazawa, S. Kinbara, A. Mishina *et al.*, J. Phys. G: Conf. Ser. **569**, 012082 (2014).

[10] A. Gal, E. V. Hungerford, and D. J. Millener, Rev. Mod. Phys. **88**, 035004 (2016).

[11] H. Lv, S. S. Zhang, Z. H. Zhang, Y. Q. Wu, J. Liu, and L. G. Cao, Chin. Phys. Lett. **35**, 062102 (2018).

[12] E. Hiyama and K. Nakazawa, Annu. Rev. Nucl. Part. Sci. **68**, 131 (2018).

[13] STAR Collaboration, Science **328**, 58 (2010); Nat. Phys. **16**, 404 (2020).

[14] PANDA Collaboration, http://www-panda.gsi.de; K.-T. Brinkmann, P. Gianotti, and I. Lehmann, Nucl. Phys. News **16**, 15 (2006).

[15] T. R. Saito, D. Nakajima, C. Rappold *et al.*, Nucl. Phys. A **881**, 218 (2012); T. R. Saito, E. Kim, and D. Nakajima, Few-Body Syst. **54**, 1211 (2013).

[16] NICA White Paper, http://theor.jinr.ru/twiki-cgi/view/NICA/WebHome.

[17] H. Tamura, Prog. Theor. Exp. Phys. **2012**, 02B012 (2012).

[18] J. C. Yang, J. W. Xia, G. Q. Xiao *et al.*, Nucl. Instrum. Methods B **317**, 263 (2013).

[19] A. S. Botvina and J. Pochodzalla, Phys. Rev. C **76**, 024909 (2007); A. S. Botvina, K. K. Gudima, J. Steinheimer *et al.*, Nucl. Phys. A **881**, 228 (2012).

[20] S. Bleser *et al.*, Phys. Lett. B **790**, 502 (2019).

[21] A. Andronic, P. Braun-Munzinger, J. Stachel, and H. Stöcker, Phys. Lett. B **697**, 203 (2011).

[22] T. Gaitanos and H. Lenske, Phys. Lett. B **737**, 256 (2014).

[23] T. Gaitanos, Ch. Moustakidis, G. A. Lalazissis, and H. Lenske, Nucl. Phys. A **954**, 308 (2016).

[24] A. S. Botvina, J. Steinheimer, E. Bratkovskaya, M. Bleicher, and J. Pochodzalla, Phys. Lett. B **742**, 7 (2015).

[25] Z. Q. Feng, Phys. Rev. C **93**, 041601(R) (2016).

[26] A. Le Fèvre, J. Aichelin, C. Hartnack, and Y. Leifels, Phys. Rev. C **100**, 034904 (2019).

[27] Z. Q. Feng, Phys. Rev. C **101**, 014605 (2020).

[28] Z. Q. Feng, Phys. Rev. C **84**, 024610 (2011); **85**, 014604 (2012).

[29] Z. Q. Feng, Nucl. Sci. Technol. **29**, 40 (2018).

[30] Z. Q. Feng, Nucl. Phys. A **919**, 32 (2013).

[31] Z. Q. Feng, W. J. Xie, P. H. Chen, J. Chen, and G. M. Jin, Phys. Rev. C **92**, 044604 (2015).

[32] G. A. Lalazissis, J. König, and P. Ring, Phys. Rev. C **55**, 540 (1997).

[33] S. Petschauer, J. Haidenbauer, N. Kaiser, Ulf-G. Meißner, and W. Weise, Eur. Phys. J. A **52**, 15 (2016).

[34] C. Samanta, P. Roy Chowdhury, and D. N. Basu, J. Phys. G: Nucl. Part. Phys. **32**, 363 (2006); C. Samanta, *ibid.* **37**, 075104 (2010).

[35] R. J. Charity *et al.*, Nucl. Phys. A **483**, 371 (1988).

[36] H. Hauser and H. Feshbach, Phys. Rev. **87**, 366 (1952).

[37] L. G. Moretto, Nucl. Phys. A **247**, 211 (1975).

[38] E. Friedman and A. Gal, Phys. Rep. **452**, 89 (2007).

[39] C. Hartnack, H. Oeschler, Y. Leifels, E. Bratkovskaya, and J. Aichelin, Phys. Rep. **510**, 119 (2012).

[40] J. Jastrzebski *et al.*, Phys. Rev. C **47**, 216 (1993).

[41] P. Hofmann *et al.*, Phys. Rev. C **49**, 2555 (1994).

[42] Y. S. Kim *et al.*, Phys. Rev. C **54**, 2469 (1996).

[43] U. Jahnke *et al.*, Phys. Rev. Lett. **83**, 4959 (1999).

[44] A. S. Botvina, J. Steinheimer, and M. Bleicher, Phys. Rev. C **96**, 014913 (2017).

[45] Y. L. Sun, A. S. Botvina, A. Obertelli, A. Corsi, and M. Bleicher, Phys. Rev. C **98**, 024903 (2018).

[46] T. Gaitanos, H. Lenske, and U. Mosel, Phys. Lett. B **675**, 297 (2009).

[47] T. Gaitanos, A. B. Larionov, H. Lenske, and U. Mosel, Nucl. Phys. A **881**, 240 (2012).